ARTICLE   OPEN

Point process microstructural model of metallic thin films with implications for coarsening

J. M. Rickman [1,2 ✉], K. Barmak[3], Y. Epshteyn [4] and C. Liu[5]

We develop a thin-film microstructural model that represents structural markers (i.e., triple junctions in the two-dimensional projections of the structure of films with columnar grains) in terms of a stochastic, marked point process and the microstructure itself in terms of a grain-boundary network. The advantage of this representation is that it is conveniently applicable to the characterization of microstructures obtained from crystal orientation mapping, leading to a picture of an ensemble of interacting triple junctions, while providing results that inform grain-growth models with experimental data. More specifically, calculated quantities such as pair, partial pair and mark correlation functions, along with the microstructural mutual information (entropy), highlight effective triple junction interactions that dictate microstructural evolution. To validate this approach, we characterize microstructures from Al thin films via crystal orientation mapping and formulate an approach, akin to classical density functional theory, to describe grain growth that embodies triple-junction interactions.

INTRODUCTION

The characterization of materials microstructure comprising a mosaic of grains and associated delimiting grain boundaries is necessary to obtain a quantitative understanding of materials behavior at the mesoscale as well as for property optimization. Most such characterizations focus on the temporal evolution of the distribution of grain sizes and shapes, as determined for example by stereology, and seek to interpret the results in terms of various models of grain growth[1–4]. A proper microstructural characterization goes beyond these grain distributions to also include the geometric information about grain boundaries. With the advent of, for example, precession-enhanced electron diffraction (PED) in the transmission electron microscope (TEM) one can now distinguish grains by their crystallographic orientations and tabulate corresponding grain-boundary character distributions (GBCD) from calculations based on extracted grain disorientation and boundary plane data.

Beyond microstructural characterization, there has also been considerable work to develop computational approaches to describe the evolution of such grain assemblages via grain growth, including for example those based on spin (e.g., Q-state Potts)[5–8] and phase-field models[9–11]. Such approaches are inherently spatially and temporally coarse grained and reflect the dynamics of constituent voxels or else an order parameter based on limited input information (e.g., grain-boundary energy). While such models have been particularly useful for capturing the essence of coarsening behavior, especially at long times, it is fair to say that they are usually phenomenological in nature and embody only minimal information from corresponding experimental systems.

More recent modeling work on grain coarsening in two dimensions has focused on the dynamics of triple junctions and grain disorientations that are associated with such boundary intersections in a grain-boundary network[12–15]. By virtue of the interconnections among boundaries that comprise the network as

well as topological constraints, these triple junctions are not independent and may therefore be viewed to a good approximation as an interacting "fluid" of points that also carry disorientation information. This model has the appealing virtue that it represents the network in terms of a simplified picture of evolving microstructural markers that can be tracked experimentally. One can then regard an ensemble of triple junctions associated with statistically equivalent microstructures under the same time and temperature conditions as constituting a marked stochastic point process[16,17] that is amenable to analysis using the tools of stochastic geometry. These tools may be employed to quantify triple-junction interactions and to assess the interdependence of the marks (i.e., disorientations), key inputs to the triple-junction model. Moreover, the grain-boundary network may be described using graph theory to summarize network topology and the disorientation environment of triple junctions.

We are motivated here, in part, by the notion that a grain-boundary network may be described in terms of its so-called triple-junction states, as embodied in a distribution function of the grain misorientations associated with each junction[18]. As noted by Adams et al., this description has the benefit that a spectral decomposition of the distribution function provides coefficients that delimit the grain-boundary configuration space[19]. Expanding on this framework, we will characterize such a network in terms of constituent triple-junction disorientations (i.e., the minimum misorientations consistent with crystal symmetry), ϕ, and, in addition, junction locations. For this purpose, we regard the collection of triple junctions in a particular microstructure as a representative configuration of a marked (non-Poisson) point process in which the marks reflect the three-grain disorientations associated with each junction[16,17]. (For simplicity, we will regard these three marks as independent even though crystallographic constraints dictate that they must, in fact, be correlated[18]). This point process is non-Poissonian owing to effective interactions between the triple junctions. From this perspective, the interfacial

[1]Department of Materials Science and Engineering, Lehigh University, Bethlehem, PA 18015, USA. [2]Department of Physics, Lehigh University, Bethlehem, PA 18015, USA. [3]Department of Applied Physics and Applied Mathematics, Columbia University, New York, NY 10027, USA. [4]Department of Mathematics, The University of Utah, Salt Lake City, UT 84112, USA. [5]Department of Applied Mathematics, Illinois Institute of Technology, Chicago, IL 60616, USA. ✉email: jmr6@lehigh.edu

free energy, the reversible work per unit area needed to create a new grain boundary[20], is reflected in the energetics that dictate the behavior of the triple-junction pair correlation function, namely a so-called potential of mean force[21] that in this context quantifies the reversible work needed to separate two tagged triple junctions. We will extract this potential from microstructural data below along with an estimate of the associated interaction potential for junctions. Thus, triple-junction energetics embody grain-boundary energetics. For reference, we note that very recent work by the authors to determine the relative grain-boundary energy distributions (GBEDs) in thin films indicates that the Herring condition is not satisfied in these systems over the time scales considered here. This condition, or another one based on triple-junction mobility may, however, be satisfied at later times[14,22].

The aforementioned marks reflect the grain-boundary disorientation distribution associated with the films. Given the cubic symmetry of Al films, disorientations are constrained to be in the range $[0°, 62.8°)$[23]. Thus, it is convenient to associate the marks with binned disorientations, and the inclusion of junction positions enables the determination of important positional correlations. For clarity, marked quantities will be denoted with Greek subscripts, with each subscript referring to the disorientations associated with one triple junction, while un-subscripted quantities will refer to the whole process without regard for marks.

In this work, we construct a microstructural model of a film that is couched in terms of grain triple junctions and associated disorientations and that is based on experimental crystal orientation mapping data obtained from thin Al films. The model is, however, quite general and may be applied to other polycrystalline systems. In this work, the thin-film data is interpreted in terms of a stochastic, marked point process that quantifies effective triple-junction interactions and network graphs. In particular, calculated quantities such as pair[24], partial pair, and mark correlation functions[17,25] along with microstructural mutual information (entropy) embody these interactions and dictate microstructural evolution.

RESULTS

Characterization

The procedure for the fabrication of the Al thin films used here is outlined in the Methods section below. For each field of view the grain orientations corresponding to each pixel are stored in a data file for subsequent interrogation. Figure 1a shows a representative microstructure for an Al film that was annealed for 150 min at a temperature $T = 400\,°C$ and Fig. 1b shows an automated trace of the grain boundaries and triple junctions resulting from our in-house code. The methodology employed in this code is also summarized in the Methods section.

Our aim here is to propose a dynamical equation for the triple junction density that is informed by the correlation functions and related quantities obtained above. For this purpose, we build on recent work[26] that describes grain growth in terms of triple-junction locations and associated disorientations. In its current form, this model lacks information regarding the interactions among triple junctions and the role of disorientations in such interactions, and we will incorporate such interactions via $F(\beta, [\rho])$ below. As noted above, it is convenient to characterize a columnar, thin-film microstructure in terms of a collection of triple points that may be identified and, ultimately, tracked experimentally. From this perspective, we regard the triple points in related microstructures (e.g., microstructures from the same sample under the same processing conditions) as the elements of an ensemble that can be described as a marked point process that may be analyzed with the associated mathematical machinery. It is important to note here that this process is assumed to be

stationary in space, with a triple-junction density that is constant for the ensemble, but not in time as the triple-junction density decreases with time during coarsening. As will be seen below, we can invoke theorems from applied mathematics to conclude that the triple-junction point process is a Gibbs point process for the aforementioned related microstructures. As such, we employ a statistical physics approach to obtain important characteristics of this process.

The simplest assumption, which we invoke here, is that triple junctions effectively interact via a pair potential that may be extracted from static correlation functions. This potential, along with a microstructural temperature, thereby determines the probability of observing a given microstructure. Moreover, we assume that these potentials may depend on the disorientations of grains that meet at the junctions and, for this reason, it is useful to mark triple junctions to distinguish among different interactions. More specifically, the triple-junction pair potential is obtained via a potential of mean force that is calculated directly from the pair correlation function and the associated direct correlation function. Under our assumptions, the pair correlation function, in turn, determines the entropy of a microstructure and thereby serves as a basis for describing the associated thermodynamics of a microstructure. Thus, these statistical quantities are convenient descriptors that are used to characterize a static thin-film microstructures. In addition, as described below, the energetic information obtained from the direct correlation function is a key input to a dynamic density function theory of grain coarsening in terms of the kinetics of triple junctions.

To quantify the effective interactions among the triple junctions in the Al thin films, we first calculate the (unmarked) pair correlation function, $g(r)$, from the triple-junction coordinates extracted from the crystal orientation maps. The grains are, to a good approximation, columnar, as has been verified in earlier studies[22,27]. For a field of view having area A, if the average number of triple junctions in a circular annulus at a distance r from a tagged point is $\langle n(r) \rangle$ and the corresponding average for uncorrelated points is $\langle n^{unc}(r) \rangle$, then the pair correlation function is proportional to the conditional probability density that a triple junction will be located at r given that another is located at the origin and is given by $g(r) = \langle n(r) \rangle / \langle n_{unc}(r) \rangle$[21]. The angle brackets denote an average over an ensemble of triple junctions. Figure 2a shows the scaled $g(r)$ for an Al film in two conditions, as deposited and annealed for 150 minutes at a temperature $T = 400°C$. For brevity, we will refer to this latter system as the annealed film hereafter. From a determination of the effective circular diameters for these conditions, it was found that the ratio of the annealed average grain area to the as-deposited area is approximately 2.1, indicating substantial coarsening. As is evident from the figure, $g(r)$, is essentially zero for small triple junction separations for both conditions and sharply peaked around $r/d(t) \approx 0.4{-}0.5$, where $d(t)$ is the time-dependent effective equivalent circle diameter of mean area. This result implies an effective repulsive interaction between triple junctions for relatively short distances and an attractive interaction at the peak locations (To quantify uncertainty estimates for $g(r)$, we considered 13 subsets of our data corresponding to portions of different fields of view. For each data subset, we calculated the corresponding pair correlation function and then examined the standard deviation of the values for each bin. From this analysis, we conclude that the small variations in the values of $g(r)$, especially in the tail, are likely due to statistical noise). Moreover, this scaling of distances in $g(r)$ with $d(t)$ suggests that triple-junction motion tracks grain growth over a broad range of time, which is essentially a consistency check of our analysis. At the latest times, grain growth stagnation is observed. Additional evidence for this tracking behavior is presented below. The peak location makes sense given that the approximate length of a side of a regular hexagon, the equilibrium two-dimensional grain shape, is $\pi d/6$. (We note that a similar calculation was done using
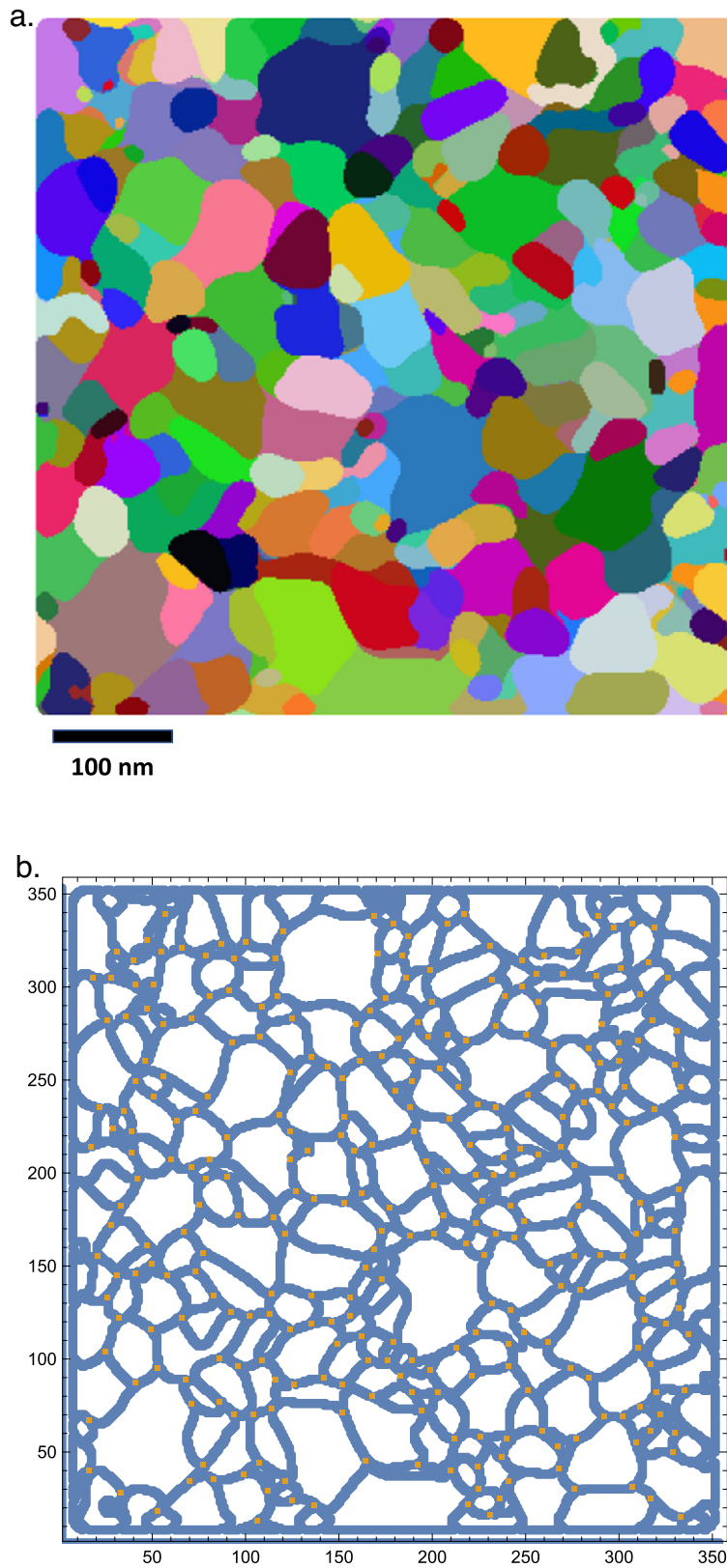
a.

100 nm

b.

Fig. 1 The microstructure for an Al film. a A representative microstructure for an Al film that was annealed for 150 min at a temperature $T = 400\,°C$. Grain colors reflect crystallographic orientations. **b** An automated trace of the grain boundaries and triple junctions corresponding to the microstructure shown in part **a**.
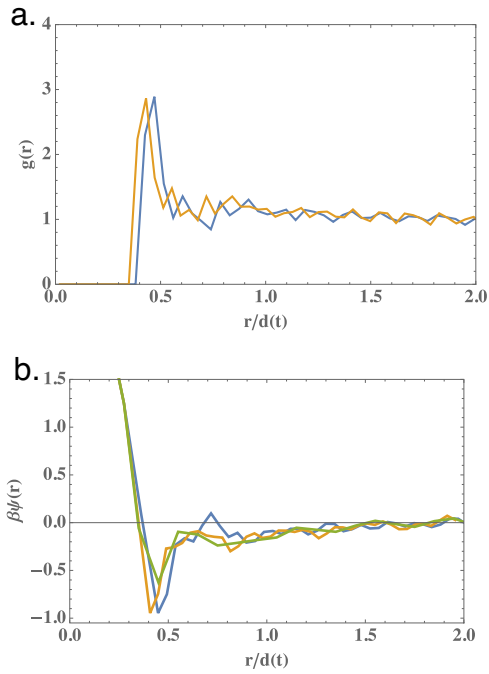
Fig. 2 The pair correlation function and associated potential of mean force. a The scaled pair correlation function, $g(r)$, versus $r/d(t)$, where r is the triple-junction separation and $d(t)$ is the time-dependent effective circular grain diameter, for an Al film in two conditions, as-deposited (blue line) and annealed for 150 minutes (gold line) at a temperature $T = 400\,°C$. **b** The corresponding reduced potentials $\beta\psi(r)$, where β places the role of an inverse temperature. For the blue and gold curves, $\psi(r) = w(r)$, the potential of mean force for the as-deposited and annealed films, respectively, while, for the green curve, $\psi(r) = u(r)$, for the annealed film. The interaction potential $u(r)$ was estimated by using the Ornstein-Zernicke integral equation[35] and the Percus–Yevick approximation.
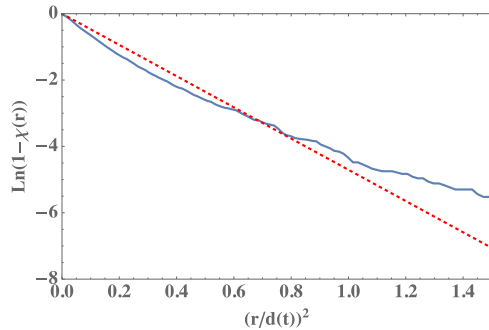

Fig. 3 The "empty-space" function for a microstructure. The function $\ln(1 - \chi(r))$ versus $r/d(t)$ for samples annealed at $T = 400\,°C$ for 150 min (blue curve) and, for comparison, for randomly-distributed triple junctions (red dashed curve).

triple junctions in synthetically generated microstructures resulting from a nucleation and growth process[28]).

Knowledge of the pair correlation function implies related knowledge of the distribution of grain sizes. To see this, consider the complementary information that may be obtained from the so-called "empty-space" function, $\chi(r)$. For an ensemble of triple junctions this function quantifies the cumulative probability of the distance from a randomly chosen point to a triple junction[29]. $\chi(r)$ is readily calculated for randomly distributed triple junctions in terms of the triple-junction density, $\rho = \langle n(r)\rangle/A$. Figure 3 shows the logarithm of the survival function, $\ln(1 - \chi(r))$, as a function of $r/d(t)$ for samples annealed at $T = 400\,°C$ for 150 min and, for

comparison, for randomly-distributed triple junctions (a Poisson process). From this figure, it is clear that the triple junctions are non-randomly distributed, as was evident from the behavior of $g(r)$. It this context, $\chi(r)$ also contains information about the distribution of grain sizes since the average reduced distance between triple junctions is given in terms of the survival function by

$$\frac{\langle r \rangle}{d} = \left(\frac{1}{d}\right) \int_0^\infty dr\,(1 - \chi(r)) \tag{1}$$

For a random distribution of triple junctions one finds that $\langle r \rangle/d = 1/\sqrt{4d^2\rho}$.

The triple-junction $g(r)$ is a key quantity that may be used to characterize a microstructure. We consider first the information content of the microstructure, as obtained from information theory[30,31]. As noted by Widom and Gao[31], the entropy of a system can be expressed in terms of an expansion in n-point distribution functions. If the interactions among triple junctions are taken to be pairwise, then the difference in entropy per triple junction between a given microstructure and one with spatially random triple points is

$$\Delta s = -\pi\rho \int_0^\infty dr\,r g(r)\ln(g(r)), \tag{2}$$

where $\rho = \langle n(r)\rangle/A$. From the perspective of information theory, Eq. (2) is the negative of the so-called mutual information[32], with the minus sign indicating that triple-point interactions lead to ordering and hence a decrease in entropy. For example, considering the system annealed at $T = 400\,°C$, using the data in Fig. 2a one finds that $\Delta s = 0.59$ nats (A nat is a natural unit of information). We note that this entropic characterization permits a direct and straightforward comparison of microstructures with a descriptor that is simpler to implement than those used for microstructural reconstruction[33].

The preceding development does not depend directly on knowledge of triple junction energetics. It is nevertheless useful to obtain interaction energy among the triple junctions. For this purpose one may take the triple-junction point process to be a Gibbs point process, consistent with the Hammersley–Clifford theorem[17]. For simplicity, we assume that the triple junctions interact via a pair potential, $u(r)$. While several fitting procedures may be used to infer the potential, we follow here an approach taken in statistical physics wherein the potential of mean force, $w(r)$, is given in terms of the pair correlation function by $\beta w(r) = -\ln g(r)$[21], where β is an effective inverse temperature of the microstructure. $w(r)$ reflects both direct and indirect triple-junction interactions and may be roughly approximated by $u(r)$ for low triple-junction densities. As noted by Vedanti et al., the microstructural temperature scale is several orders of magnitude higher than that associated with typical thermal processes[34]. Figure 2b shows $\beta w(r)$ as a function of $r/d(t)$ for both the as-deposited and annealed Al films that highlight the attractive interactions. The grain-boundary energy scale embodied in $w(r)$ should be similar to the microstructural "thermal" energy scale, $1/\beta$, given that coarsening readily occurs over the time scales monitored here. Indeed, the reduced potential of mean force, $\beta w(r)$, shown in Fig. 2b has an attractive well with a depth of ~0.9.

To obtain a somewhat better estimate of $u(r)$, it is useful to extract from $g(r)$ the direct correlations between triple junctions, as embodied in the correlation function $c^{(2)}(r)$. This correlation function may be calculated from the pair correlation function $g(r)$ using the Ornstein-Zernike equation[35] that, for a homogeneous, isotropic system, is given by the integral equation

$$h(|\mathbf{r} - \mathbf{r}'|) = c^{(2)}(|\mathbf{r} - \mathbf{r}'|) + \rho \int d^2r''\, c^{(2)}(|\mathbf{r} - \mathbf{r}''|)\, h(|\mathbf{r}'' - \mathbf{r}'|),$$
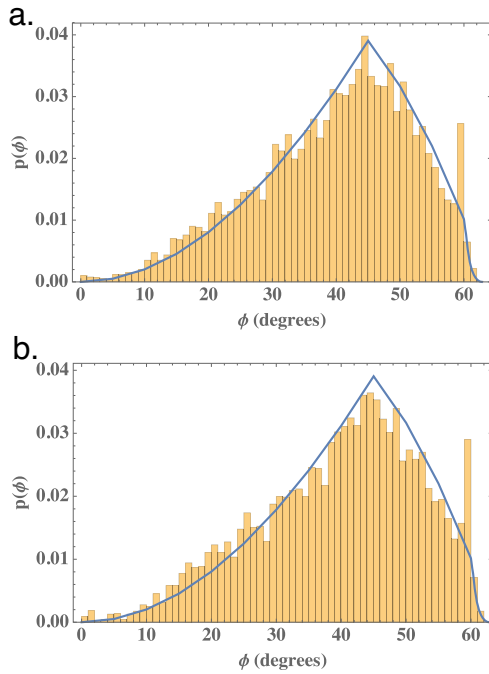
$$\tag{3}$$

Fig. 4 The triple-junction disorientation distribution function for as deposited and annealed films. a The probability density function, $p(\phi)$, for triple-junction disorientation, ϕ, for as deposited Al films (histogram). Also shown is the theoretical probability density function for randomly oriented grains in a cubic system (blue line), as determined by MacKenzie[23]. Note the texturing that is evident for $\phi \approx 60°$, corresponding to a twin. **b** The same as for part **a.**, except for the annealed film.

where $h(|\mathbf{r} - \mathbf{r}'|) = g(|\mathbf{r} - \mathbf{r}'|) - 1$ and ρ is assumed to be spatially uniform. This equation is most readily solved for $c^{(2)}(|\mathbf{r} - \mathbf{r}'|)$ via Fourier transformation. An estimate of $u(r)$ can then be obtained from the Percus–Yevick equation that is given in terms of $c^{(2)}(r)$ by

$$c^{(2)}(r) \approx [1 - \exp(\beta u(r))] g(r) \qquad (4)$$

Figure 2b also shows $\beta u(r)$ as a function of $r/d(t)$ for the annealed Al film as obtained from this procedure. As is evident from the figure, there is only a small difference between $u(r)$ and $w(r)$ at these triple-junction densities. Finally, we note that the direct correlation function is also the main ingredient in a classical density functional theory of triple-junction motion, as discussed below.

Before looking at other correlations in detail, it is useful to examine the distribution of disorientations in the thin-film microstructures. This distribution may be summarized in the form of a probability density function, $p(\phi)$, of disorientations associated with the triple junctions, as shown in Fig. 4 for both the as-deposited and the annealed films. As can be seen from the figures and a comparison with the Mackenzie distribution for randomly disoriented cubes[23] that is also presented, the disorientation distributions are consistent with the random (i.e., Mackenzie) distribution for both films, except for $\phi \approx 60°$. This result is perhaps not too surprising given that $\phi = 60°$ corresponds to a (low-energy) twin boundary. While these plots convey disorientation frequency and highlight texture, they do not reveal any spatial correlations among grain-boundary disorientations. Such correlations may be revealed by marking the triple junctions to summarize associated disorientations and then examining spatial associations between triple junctions.

The interactions between marked triple-junctions can be deduced from the partial pair correlation functions, $g_{\alpha\beta}(r)$, where
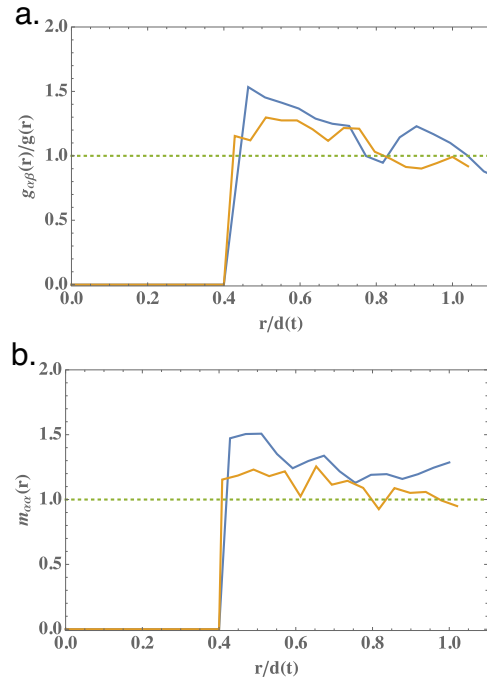

Fig. 5 The partial and mark correlation function for triple junctions. a The correlation function ratio, $g_{\alpha\beta}(r)/g(r)$, versus $r/d(t)$ for Al films under the same conditions as listed in Fig. 1a. The disorientations, ϕ, considered here are in the interval [55.0°, 61.0°]. The relative partial pair correlation function for disorientations close to the twin disorientation of 60° do not indicate strong spatial correlations, suggesting that the associated grain boundaries are essentially randomly distributed in the microstructure. The as-deposited (annealed) results are shown in blue (gold). **b** The mark correlation function, $m_{\alpha\alpha}(r)$, versus $r/d(t)$ for Al films under the same conditions as listed in Fig. 1a. ϕ is in the interval [50.0°, 60.0°].

α and β are marks denoting disorientation ranges, and we will bin disorientations in either 5° or 10° intervals (i.e., $\alpha, \beta = 1, 2, \cdots, 12$ or $1, 2, \cdots 6$) depending upon the granularity of information desired. By analogy with the statistical mechanics of fluid mixtures[36], one can regard these marks as akin to different "chemical species" in a multi-component fluid. These correlation functions may be calculated for a point process comprising n triple junctions located at positions $\mathbf{r}_i (i = 1, 2, 3, \cdots, n)$ from the relation

$$p_i p_j \frac{g_{\alpha\beta}(r)}{g(r)} = \frac{\sum_{i=1}^{n} \sum_{j=1}^{n} (1 - \delta_{ij}) C_{\alpha\beta}(\mathbf{r}_i, \mathbf{r}_j) k(|\mathbf{r}_i - \mathbf{r}_j| - r)}{\sum_{i=1}^{n} \sum_{j=1}^{n} (1 - \delta_{ij}) k(|\mathbf{r}_i - \mathbf{r}_j| - r)} = \langle C_{\alpha\beta}(\mathbf{r}_i, \mathbf{r}_j) \rangle_r,$$

$$(5)$$

where $C_{\alpha\beta}(\mathbf{r}_i, \mathbf{r}_j)$ is a test function that is one if point i (j) corresponds to mark type $\alpha(\beta)$, $k(|\mathbf{r}_i - \mathbf{r}_j| - r)$ is a kernel function that is one if the inter-point separation is within a narrow circular annulus at r and p_i is the proportion of triple points of type i. The angle brackets with subscript r indicate that this ratio may be regarded as an average over pairs of triple junctions separated by a distance r[25].

As an illustration of the behavior of this correlation function ratio, Fig. 5a shows the dependence of $g_{\alpha\beta}(r)/g(r)$, on $r/d(t)$ for Al films in the previously described as deposited and annealed conditions for ϕ in [55.0°, 61.0°]. Deviations from unity near $r/d(t)$ indicate stronger attractive interactions between triple junctions in this disorientation range relative to the unmarked process, with the as-deposited film evincing a slightly stronger interaction strength (To assess the related uncertainties in the correlation function ratio, we examined the data for the annealed sample as the deviation from randomness is smaller here. For this data, we calculated the standard deviation of the mean for the correlation

function ratio near $r/d(t) = 0.5$ and found that the relative error in this ratio is ~12%. Thus, these results for both the as-deposited and the annealed sample are both significant; recognizing that, in the case of the annealed sample, we are inferring a small correlation). It should be noted that one contribution to the nearest-neighbor interaction is simply due to the fact that two neighboring triple junctions are joined by the same grain boundary. Once the partial pair correlation functions are determined, it is also possible then to isolate the individual entropic contributions of the disorientation ranges to the total mutual information defined above by analogy with a formalism used to compute the entropy of a multi-component fluid[37]. This procedure requires a weighted decomposition of $g(r)$ in terms of the $g_{\alpha\beta}(r)$ and is somewhat more complicated here owing to the fact that three grains meet at a triple junction.

To probe further relationships between marks, Fig. 5b displays the mark correlation function

$$m_{aa}(r) = \frac{\langle \mu_{aa}(\mathbf{r}_i, \mathbf{r}_j)\rangle_r}{\langle \mu_{aa}^{unc}\rangle} \tag{6}$$

where $\mu_{\alpha\beta}(\mathbf{r}_i, \mathbf{r}_j)$ is the product of the number of disorientation angles of type α at triple junctions located at positions $\mathbf{r}_i$ and $\mathbf{r}_j$, $r = |\mathbf{r}_i - \mathbf{r}_j|$ and $\mu_{\alpha\beta}^{unc}$ is the corresponding quantity if the marks are spatially uncorrelated. As is evident from the figure, there is some degree of spatial correlation between the number of marks per triple junction for nearby triple junctions. As noted above for $g(r)$, the scaling of the pair correlation functions and the mark correlation function with $d(t)$ indicates that triple-junction motion tracks grain growth over a broad range of time.

Finally, additional information can be garnered from a graphical analysis of the grain-boundary network, a collection of interconnected grain boundaries and triple junctions. Figure 6a shows this network for the microstructure shown in Fig. 1a. The boundaries are color coded to highlight different disorientation bins, each bin corresponding to a sequential 10°-interval for $0° \leq \phi \leq 60.0°$. From the perspective of graph theory, the grain-boundary network is a graph in which the triple junctions are vertices of degree three (apart from edge effects) and the boundaries comprise weighted edges. Thus, this graph also provides a visual representation of the edge weight spectrum shown in Fig. 4b. It is convenient to examine a sub-network comprising only boundaries corresponding to a particular disorientation bin. Figure 6b shows such a structure for disorientations $50.0° \leq \phi \leq 60.0°$ in which constituent segments are color-coded by length. Clearly, there is a distribution of segment lengths, and one can characterize this distribution by its dispersity index[38], Đ, (a disorientation "fingerprint"). For all of the disorientation bins considered here, there is little dispersity variability as $1.55 \leq Đ \leq 1.61$.

Grain growth model

The structural information embodied in the pair correlation functions outlined above may be used to inform a grain-growth model couched in terms of triple-junction energetics. For this purpose, we employ an approach similar to that used in classical dynamic density functional theory (DDFT), a close cousin of the phase-field model, to describe junction kinetics[39]. In this formalism the evolution of a system is determined by a phenomenological equation of motion based on a truncated functional expansion of the free energy[40] of a "slow" variable. For simplicity, we will not distinguish among disorientations here and focus on the total triple-junction density $\rho(\mathbf{r}, t)$ at position $\mathbf{r}$ at time t. We consider first the bulk case. The corresponding Helmholtz free energy, $F(\beta, [\rho])$, for inverse microstructural temperature β comprises two parts, namely:

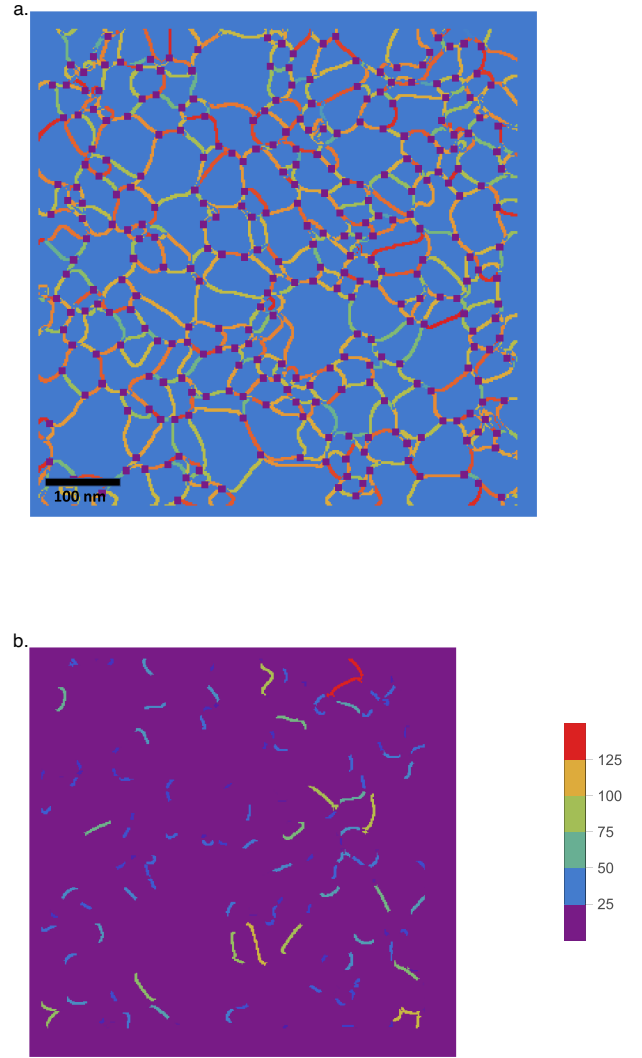$$F(\beta, [\rho]) = F_{id}(T, [\rho]) + F_{exc}(T, [\rho]) + F_{ext}(T, [\rho]), \tag{7}$$

Fig. 6 A grain-boundary network with disorientations highlighted. a The grain-boundary network with associated boundary disorientations (color coded) and triple junctions for the microstructure shown in Fig. 1a. **b** The grain boundary segments with disorientations $50.0° \leq \phi \leq 60.0°$. Segments are color coded by length, with the longer segments shaded towards the red end of the color spectrum as indicated in the legend (by length in pixels).

where the ideal gas and interaction terms are given, respectively, by

$$F_{id}(\beta, [\rho]) = \tfrac{1}{\beta} \int d^2r \left(\rho(\mathbf{r}, t) \ln(\Lambda^3 \rho(\mathbf{r}, t)) - 1 \right),$$

$$F_{exc}(\beta, [\rho]) = -\tfrac{1}{2\beta} \int \int d^2r \, d^2r' \, c^{(2)}(\mathbf{r} - \mathbf{r}') \delta\rho(\mathbf{r}) \delta\rho(\mathbf{r}'), \tag{8}$$

$$F_{ext}(T, [\rho]) = \psi_0 \int d^2r \, \rho(\mathbf{r}).$$

where Λ is the thermal deBroglie wavelength, $c^{(2)}(\mathbf{r} - \mathbf{r}')$ is the direct correlation function containing experimental information as described above and ψ_0 is a (positive) energy penalty for the presence of triple junctions. Equation (7) is a functional Taylor expansion of the free energy about a homogeneous system with uniform junction density reference density ρ_0.

Our aim here is to propose a dynamical equation for the triple junction density that is informed by the correlation functions and related quantities obtained above. For this purpose, we build on recent work[26] that describes grain growth in terms of triple-junction locations and associated disorientations. In its current form, this model lacks information regarding the interactions
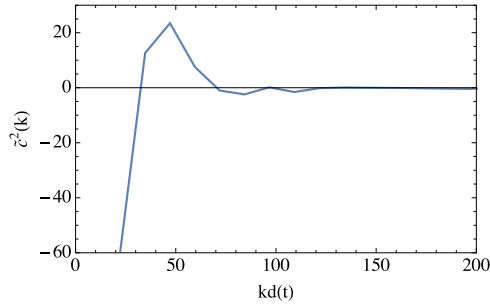
Fig. 7 The direct correlation function for triple junctions. The Fourier transform of the direct correlation function, $\tilde{c}^{(2)}(k)$, versus $kd(t)$ for the Al microstructures annealed for 150 minutes at $T = 400\,°C$.

among triple junctions and the role of disorientations in such interactions, and we will incorporate such interactions via $F(\beta, [\rho])$ below. From this perspective, the approach outlined below is akin to Model A of critical dynamics[41] for a non-conserved order parameter.

As $\rho(\mathbf{r}, t)$ is a non-conserved parameter, we can write a noise-free, dynamical equation for this coarse-grained parameter as

$$\frac{\partial \rho}{\partial t} = -L \frac{\delta F[\rho]}{\delta \rho(\mathbf{r}, t)}, \qquad (9)$$

where L is a kinetic coefficient. Equation (9) may be solved numerically. It is useful though to examine first junction dynamics for perturbations from a homogeneous reference state[42]. In particular, the linearized triple-junction dynamics relative to a spatially homogeneous triple-junction "fluid" may be obtained by taking $\rho(\mathbf{r}, t) = \rho_0 + \delta\rho(\mathbf{r}, t)$. One finds that

$$\left(\frac{\beta}{L}\right)\frac{\partial}{\partial t}\delta\rho = -\left[\delta\rho - \rho_0 \int d^2r'\, c^{(2)}(|\mathbf{r} - \mathbf{r}'|)\delta\rho(\mathbf{r}')\right], \qquad (10)$$

assuming translational and rotational invariance. By Fourier transforming Eq. (10) one finds that

$$\delta\tilde{\rho}(\mathbf{k}, t) = \delta\tilde{\rho}(\mathbf{k}, 0)\,\exp[\lambda(k)t], \qquad (11)$$

where the decay rate

$$\lambda(k) = \frac{L}{\beta}\left(\rho_0\,\tilde{c}^{(2)}(k) - 1\right) \qquad (12)$$

and the tilde denotes a Fourier transform.

The decay rate $\lambda(k)$ determines the stability of the homogeneous "fluid" of triple junctions such that small perturbations corresponding to $\lambda(k) > 0$ (< 0) are unstable (stable). It should be noted that the direct correlation function is implicitly a function of ρ_0 and so the marginal stability condition depends on whether the microstructure has a large (small) ρ_0 corresponding to small (large) grains. For example, the Fourier transform, $\tilde{c}^{(2)}(k)$, as obtained by the Fourier transform of the Ornstein-Zernike relation (see Eq. (3)), is shown in Fig. 7 for the low-ρ_0 annealed Al microstructures discussed above. Therefore, as a microstructure coarsens, there can be attendant changes in $\tilde{c}^{(2)}(k)$ associated with a net decrease in ρ_0.

To illustrate the dynamics of the coarse-grained triple-junction density, we numerically integrated the equation of motion (Eq. (9)) and tracked the total number of triple junctions, $N(t)$, present in the system at time t. For concreteness, a Gaussian distribution of initial triple-junction densities was chosen with the ratio of the standard deviation to the average density equal to 0.25. The microstructural temperature was taken as 3.0 times the potential energy scale, and the integration time step Δt was chosen to be $0.001\,L^{-1}$, where L is the phenomenological mobility parameter. Figure 8 below shows the resulting fraction of triple junctions, $N(t)/N(t = 0)$, as a function of t, for two different values of the
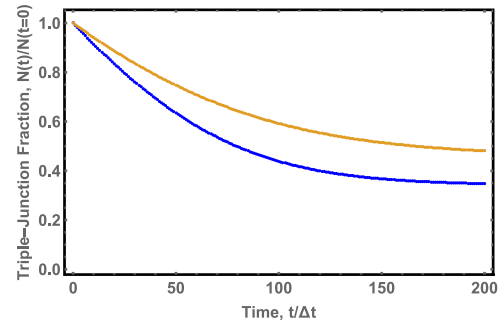

Fig. 8 The time dependence of the coarse-grained triple-junction fraction for an evolving microstructure. The evolution of the triple-junction fraction, $N(t)/N(t = 0)$, as a function of reduced time, Δt, for the coarse-grained grain-growth model for two applied fields, $\psi_0 = 1.0$ (blue) and $\psi_0 = 3.0$ (gold). The applied field leads to a reduction in the triple-junction fraction and partially controls the rate of reduction.

external field, ψ_0. As is evident from the figure, the fraction of triple junctions in the system decreases with time with a rate that is partially controlled by the external field.

Finally, for a thin film, in addition to the impact of the free surface and the substrate interface on the direct correlation function, one can incorporate a field, $\Psi(\mathbf{r})$, into the external free energy such that it is redefined to be

$$F_{ext}(T, [\rho]) = \int d^2r\, \rho(\mathbf{r})[\psi_0 + \Psi(\mathbf{r})]. \qquad (13)$$

This additional field models the spatial variation of the triple-junction density in the film resulting from interfacial boundary conditions. For sufficiently thick films with a normal in the z-direction, it may be deduced from $\rho(z)$ as obtained from two-dimensional slices through the microstructure. We also note that the energy penalty ψ_0 can be tuned to determine the number of triple junctions in the system at late time and thereby incorporate grain stagnation into the model.

Discussion

In this work, we developed a microstructural model for thin films in which triple junctions are described in terms of a stochastic, marked point process and the associated microstructure in terms of a grain-boundary network. This model was then employed to characterize microstructures obtained from experimental crystal orientation mappings of thin metallic (i.e., Al films), with the resulting picture of an ensemble of interacting triple junctions used to inform grain-growth models with experimental data. The triple-junction point process is characterized by calculated quantities such as pair, partial pair, and mark correlation functions, along with the microstructural mutual information (entropy). From these quantities, one can then infer associated triple-junction interaction energies and their impact on microstructural evolution.

Several insights have been garnered from this work. First, our analysis suggests that triple-junction motion tracks grain growth over at least most of the time scale explored in this study. This suggestion is borne out in the results that show that the pair correlation distances scale with the time-dependent grain diameter, $d(t)$. Next, the grain-boundary energy scale embodied in $w(r)$ should be similar to the microstructural "thermal" energy scale, $1/\beta$, given that coarsening readily occurs over a relevant time scale. It was, in fact, found that $\beta w(r)$ has an attractive well with a depth of ~0.9. We note that this information is difficult to obtain via other means, such as a grain-boundary grooving study and, as described above, the associated direct correlation function is a key input to a dynamic density functional theory of triple-junction kinetics. Finally, with regard to texturing in the annealed

films, the relative partial pair correlation function for disorientations close to the twin disorientation of 60° does not evince strong spatial correlations, suggesting that the associated grain boundaries are essentially randomly distributed in the microstructure.

Our formulation of the approximate microstructural entropy change, $\Delta s(\rho)$, couched conveniently in terms of the triple-junction density, ρ (see Eq. (2)), serves as a starting point for the development of a "thermodynamics" of coarsening. We note that other authors have used the Shannon entropy with a probability calculated from a grain-size distribution to define a microstructural temperature, T[34]. In our development, for example, we can approximate the entropy by $s(\rho) \approx s_0(\rho) + \Delta s(\rho)$, where $s_0(\rho)$ is the reference entropy associated with randomly distributed points and define a corresponding microstructural pressure $P = T \partial s(\rho)/\partial(1/\rho)$. Since ρ decreases during coarsening and s decreases concomitantly, one expects that $P < 0$. Moreover, response functions, such as microstructural compressibility, can be calculated from higher-order derivatives of the entropy.

Given the formalism described here, there are several fruitful directions for ongoing work. First, it is of interest to obtain a more complete picture of the temporal evolution of coarsening in terms of both triple-junction positions and grain disorientations. In thin films, this process may be somewhat complex owing to growth stagnation at late times. We are currently working to acquire more microstructural data for Al thin films at different temperatures for this purpose. In addition, we will wish to examine other thin-film systems, and we have begun a triple-junction analysis of Pd thin films. Second, it would be informative to establish a more direct connection between our results and recent thermodynamic descriptions of microstructural evolution[34], especially the microstructural temperature, as highlighted above. Third, once we have additional experimental microstructural data at different annealing times, our aim is to track triple-junction motion to quantify directly triple-junction dynamics. It is expected that non-equilibrium correlation functions of the triple-junction density at spatial positions $\mathbf{r}$ and $\mathbf{r}'$, such as $\langle \rho(\mathbf{r}, t)\rho(\mathbf{r}', t)\rangle$, will embody the dynamics at time t. Using this information, we expect to obtain a more complete, physical picture of triple-junction motion that will inform the development of an ongoing, related modeling effort[26]. Finally, we wish to compare the results of our proposed DDFT grain growth model with spin (e.g., Q-state Potts)[5–8] and phase-field models[9–11]. As noted above, our approach is sufficiently flexible to incorporate grain-boundary stagnation at late times, an important phenomenon in thin-film systems that is often omitted in other treatments. This comparison is also the subject of ongoing work.

METHODS

Sample preparation and crystal orientation mapping

Details of film deposition, annealing and crystal orientation mapping and cleanup are given elsewhere[27,43]. Briefly, a 100 nm-thick Al film was sputter deposited onto a thermally oxidized Si wafer, and was annealed at 400 °C for 30 min and 150 min in a flowing Ar-H$_2$ environment[27]. To achieve electron transparency, all sample substrates were back-polished and then chemically back-etched using a hydrofluoric and nitric acid solution, as described in refs. [44,45]. Crystal orientation mapping of the samples was done with precession-enhanced electron diffraction (PED) with a precession angle of 0.6°. The mapping was performed on square grids with step sizes of 4 nm for the as-deposited film and 5 nm for the annealed films. The collected patterns were assigned crystal orientations using the ASTAR® system (NanoMEGAS, Brussels, Belgium)[27]. These orientation data were converted to a hexagonal grid, imported into TSL OIM® 8.1 (EDAX, Mahwah, NJ, USA) and cleaned up. First, grains were defined to be clusters of points within 5° disorientation of one

another, then performing a dilation step to eliminate those grains smaller than 5% of the mean grain area (calculated before cleanup). After assigning a single average orientation to each grain, the data were subject to a pseudosymmetry cleanup. This step corrects regions with data points whose diffraction patterns are related by certain 180° symmetry operations, and are falsely assigned different orientations[43,46]. Finally, the orientation data were exported on the original square grids.

Analysis

Given the aforementioned PED data for approximately sixteen microstructures for each time (i.e., two distinct microstructures from eight separate fields of view), we employed an in-house code to locate the triple-junctions and associated grain disorientations in each microstructure. This analysis required the elimination of spurious pixels comprising fictitious grains located at grain boundaries by the re-assignment of the corresponding pixel orientations to those of neighboring "large" grains. Moreover, to prevent the identification of spurious triple junctions with our procedure, we eliminated some triple junctions that were below a (small) cut-off distance from other junctions. This procedure results in a very minor bias in the calculation of the triple-junction pair correlation functions at small separation. Grain disorientations are readily obtained by first converting the Euler angles quantifying each grain orientation to the equivalent quaternion representation and then computing boundary misorientations using quaternion algebra. The corresponding disorientations are then determined by applying cubic symmetry operations to each misorientation to find the misorientation having the minimum angle[47]. We note that degrees of freedom associated with, for example, rotation axes are not incorporated (yet) in our analysis as we believe that it is useful to begin with a description based on the disorientation angle rather than analyzing correlations in a high-dimensional space. The dimensional reduction focusing on disorientation angles is a practical compromise.

From the resulting list of triple-junction coordinates and associated grain disorientations, we calculated the various correlation functions, etc., described above. To obtain statistically significant results, these quantities were averaged over an ensemble of microstructural data corresponding to the same annealing temperature and time (i.e., the relevant fields of view).

DATA AVAILABILITY

The authors will make available, upon request, the data used in this work. It is understood that the data provided will not be for commercial use.

CODE AVAILABILITY

The authors will make available, upon request, the code used in the applications described in this work. It is understood that the code will not be for commercial use.

REFERENCES

1. Carpenter, D. T., Rickman, J. M. & Barmak, K. A methodology for automated quantitative microstructural analysis of transmission electron micrographs. *J. Appl. Phys.* **84**, 5843–5854 (1998).
2. Chinn, R. Grain sizes of ceramic by automated image analysis. *J. Am. Ceram. Soc.* **77**, 589–592 (1994).
3. Peregrina-Barreto, H. et al. Automatic grain size determination in microstructures using image processing. *Measurement* **46**, 249–258 (2013).
4. Barmak, K. et al. Grain growth and the puzzle of its stagnation in thin films: the curious tale of a tail and an ear. *Prog. Mater. Sci.* **58**, 987–1055 (2013).

5. Anderson, M. P., Srolovitz, D. J., Grest, G. S. & Sahni, P. S. Computer simulation of grain growth: I. Kinetics. *Acta Metall.* **32**, 783–791 (1984).

6. Sahni, P. S., Grest, G. S., Anderson, M. P. & Srolovitz, D. J. Kinetics of the Q-state Potts model in two dimensions. *Phys. Rev. Lett.* **50**, 263–266 (1983).

7. Frazier, W. E., Rohrer, G. S. & Rollett, A. D. Abnormal grain growth in the Potts model incorporating grain boundary complexion transitions that increase the mobility of individual boundaries. *Acta Mater.* **96**, 390–398 (2015).

8. Marvel, C. J. et al. Relating the kinetics of grain-boundary complexion transitions and abnormal grain growth: a Monte Carlo time-temperature-transformation approach. *Acta Mater.* **239**, 118262 (2022).

9. Krill, C. E. III & Chen, L.-Q. Computer simulation of 3-D grain growth using a phase-field model. *Acta Mater.* **50**, 3059–3075 (2002).

10. Moelans, N., Blanpain, B. & Wollants, P. A phase field model for the simulation of grain growth in materials containing finely dispersed incoherent second-phase particles. *Acta Mater.* **53**, 1771–1781 (2005).

11. Chen, L.-Q. Phase-field models for microstructure evolution. *Annu. Rev. Mater. Res.* **32**, 113–140 (2002).

12. Barmak, K. et al. Critical events, entropy, and the grain boundary character distribution. *Phys. Rev. B* **83**, 134117 (2011).

13. Bardsley, P. et al. Towards a gradient flow for microstructure. *Atti Accad. Naz. Lincei Rend. Lincei Mat. Appl.* **28**, 777–805 (2017).

14. Epshteyn, Y., Liu, C. & Mizuno, M. Motion of grain boundaries with dynamic lattice misorientations and with triple junctions drag. *SIAM J. Math. Anal.* **53**, 307 (2021).

15. Epshteyn, Y., Liu, C. & Mizuno, M. Large time asymptotic behavior of grain boundaries motion with dynamic lattice misorientations and with triple junctions drag. *Commun. Math. Sci.* **19**, 1403–1428 (2021).

16. Diggle, P. J. Statistical Analysis of Spatial and Spatio-Temporal Point Patterns, (CRC Press, 2014).

17. Baddeley, A., Rubak, E., & Turner, R. Statistical Point Patterns: Methodology and Applications in R. (CRC Press, 2016).

18. Johnson, O. K. & Schuh, C. A. The triple junction hull: tools for grain boundary network design. *J. Mech. Phys. Solid* **69**, 2–13 (2014).

19. Adams, B. L., Kalidindi, S. R. & Fullwood, D. T. Microstructure-Sensitive Design for Performance Optimization. First edition. (Butterworth-Heinemann, 2012).

20. Gao, X. & Huang, Z. P. Surface/interfacial energy theory of solids. In: Altenbach, H., Öchsner, A. (eds) Encyclopedia of Continuum Mechanics (Springer, 2020).

21. Chandler, D. Introduction to Modern Statistical Mechanics (Oxford University Press, 1987).

22. Patrick, M. et al. Relative grain boundary energies from triple junction geometry: limitations to assuming the Herring condition in nanocrystalline thin films. *Acta Mater.* **242**, 118476 (2023).

23. Mackenzie, J. K. Second paper on statistics associated with the random disorientation of cubes. *Biometrika* **45**, 229–240 (1958).

24. Torquato, S. Random Heterogeneous Materials: Microstructure and Macroscopic Properties (Springer-Verlag, 2002).

25. Wiegand, T. & Moloney, K. A. Estimators and toolbox in Handbook of Spatial Point-Pattern Analysis in Ecology (CRC Press, 2013).

26. Epshteyn, Y., Liu, C. & Mizuno, M. A stochastic model of grain boundary dynamics: A Fokker-Planck perspective. *Math. Models Methods Appl. Sci.* **32**, 2189–2236 (2022).

27. Rohrer, G. S. et al. The grain boundary character distribution of highly twinned nanocrystalline thin film aluminum compared to bulk microcrystalline aluminum. *J. Mater. Sci.* **52**, 9819–9833 (2017).

28. Tong, W. S., Rickman, J. M. & Barmak, K. Quantitative analysis of spatial distribution of nucleation sites: microstructural implications. *Acta Mater.* **47**, 435–445 (1999).

29. Baddeley, A. Spatial point processes and their applications. In: Weil, W. (eds) Stochastic Geometry. Lecture Notes in Mathematics (Springer, 2007).

30. Gray, R. M. Entropy and Information Theory (Springer-Verlag, 1990).

31. Widom, M. & Gao, M. First principles calculation of the entropy of liquid aluminum. *Entropy* **21**, 131 (2019).

32. Cover, T. M. & Thomas, J. A. Elements of Information Theory (John Wiley and Sons, 1991).

33. Piasecki, R. Microstructure reconstruction using entropic descriptors. *Proc. R. Soc. A* **467**, 806–820 (2011).

34. Vedanti, P., Wu, X. & Berdichevsky, V. Entropy decay during grain growth. *Sci. Rep.* **10**, 11912 (2020).

35. He, Y., Rice, S. A. & Xu, X. Analytic solution of the Ornstein-Zernike relation for Inhomogeneous liquids. *J. Chem. Phys.* **145**, 234508 (2016).

36. Matteoli, E. & Mansoori, G. A. A simple expression for radial distribution functions of pure fluids and mixtures. *J. Chem. Phys.* **103**, 4672–4677 (1995).

37. Gao, M. C. & Widom, M. Information entropy of liquid metals. *J. Phys. Chem. B* **122**, 3550–3555 (2018).

38. Stepto, R. F. T. et al. Dispersity in polymer science. *Pure Appl. Chem.* **81**, 351–353 (2009).

39. te Vrugt, M., Löwen, H. & Wittkowski, R. Classical dynamical density functional theory: from fundamentals to applications. *Advances in Physics* **69**, 121–247 (2020).

40. Ramakrishnan, T. V. & Yussouff, M. First-principles order-parameter theory of freezing. *Phys. Rev. B* **19**, 2775 (1979).

41. Hohenberg, P. C. & Halperin, B. I. Theory of dynamic critical phenomena. *Rev. Mod. Phys.* **49**, 435–479 (1977).

42. Onuki, A. Phase Transition Dynamics (Cambridge University Press, 2002).

43. Patrick, M. J. et al. Relative grain boundary energies from triple junction geometry: limitations to assuming the Herring condition in nanocrystalline thin films (submitted for publication).

44. Yao, B. et al. A modified back etch method for preparation of plan-view high-resolution transmission electron microscopy samples. *J. Electron Microsc.* **55**, 209–214 (2006).

45. Yao, B. & Coffey, K. R. Back-etch method for plan view transmission electron microscopy sample preparation of optically opaque films. *J. Electron Microsc.* **57**, 47–52 (2008).

46. Liu, X. et al. Comparison of crystal orientation mapping-based and image-based measurement of grain size and grain size distribution in a thin aluminum film. *Acta Mater.* **79**, 138–145 (2014).

47. Rowenhorst, D. et al. Consistent representations of and conversions between 3D rotations. *Model. Simul. Mater. Sci. Eng.* **23**, 083501 (2015).

AUTHOR CONTRIBUTIONS

J.M.R. is the primary author (and guarantor) of this work. He performed most of the data analysis. K.B. and her students obtained the crystal orientation mapping data used in our analysis and also assisted with the data analysis, while Y.E. and C.L. developed the triple-junction grain growth model that is discussed here.

COMPETING INTERESTS

The authors declare no competing interests.

ADDITIONAL INFORMATION

Correspondence and requests for materials should be addressed to J. M. Rickman.

Reprints and permission information is available at http://www.nature.com/reprints

Publisher's note Springer Nature remains neutral with regard to jurisdictional claims in published maps and institutional affiliations.